Weather and
Climate Dynamics

Open Access

EGU

Benefits of kilometer-scale climate modeling for winds in complex terrain: strong versus weak winds

Danijel Belušić[1,2] **and Petter Lind**[1]

[1]Swedish Meteorological and Hydrological Institute (SMHI), Rossby Centre, Norrköping, 601 76, Sweden
[2]Department of Geophysics, Faculty of Science, University of Zagreb, Zagreb, 10000, Croatia

Correspondence: Danijel Belušić (danijel.belusic@smhi.se)

Abstract. The existence of many different wind types in complex terrain and the difficulty of obtaining representative wind observations hinder the analysis of the general benefits of high-resolution climate modeling for winds. We show that the added value of kilometer (km)-scale modeling is particularly pronounced in mountainous terrain and increases substantially with wind speed, with the km-scale model and observations reaching twice larger speeds than a coarser model with 12 km grid spacing. At the same time, synoptically calm conditions are prone to local thermally generated circulations, such as slope flows with typically weak winds, whose modeling results can also be considerably affected by the model resolution. We therefore focus on the mountainous region of the southern Scandinavian Mountains and analyze the winds at two ends of the wind distribution: very strong winds, generally forced by large-scale weather systems, and local, thermally generated winds in synoptically calm conditions. Strong winds in the present climate are influenced more by the terrain height and high model resolution than by the large-scale forcing, while the future change is mostly governed by the global-model large-scale circulation change. For the thermal circulations in summer, in contrast to the coarse model, the km-scale model captures glacier downslope wind in the high mountains and the resulting convergence zone as well as the increased cloud cover where the glacier wind meets the daytime upslope wind. The future change in thermal circulations is primarily influenced by the future temperature change and the high model resolution. Because the future temperature changes are considerably less uncertain than the changes in large-scale circulation, the future of local thermal circulations can be estimated with less uncertainty compared to stronger winds.

1 Introduction

Most studies dealing with kilometer (km)-scale, or convection-permitting, regional climate models (CPMs) have focused on precipitation and the associated mechanisms, especially in the present climate (e.g., Berthou et al., 2020; Ban et al., 2021). The considerable added value of CPMs compared to their parent regional climate models (RCMs) or global climate models (GCMs) is well established in the present climate for convective precipitation, especially for sub-daily heavy precipitation events (e.g., Prein et al., 2015; Lind et al., 2020; Ban et al., 2021; Lucas-Picher et al., 2021).

Studies on CPM winds, and especially their future changes, are less common. One reason for this is that winds generated or influenced by heterogeneous terrain often scale with the spatial dimensions of terrain features. In the complex terrain of the Scandinavian Mountains, which is the focus of this study, many spatial scales interact, as do the different types of terrain-induced circulations. The general difficulty of measuring the representative wind speed and direction for a certain area becomes even more apparent in such complex terrain. Therefore, evaluating the performance of km-scale regional climate models in reproducing wind is challenging, and climate modeling studies have addressed wind much less frequently compared to other variables such as temperature and precipitation. However, it has been shown that km-scale resolution is required in complex terrain to adequately simulate observed wind patterns (e.g., Wang et al., 2013; Cholette et al., 2015; Belušić et al., 2018; Belušić Vozila et al., 2024; Molina et al., 2024). Furthermore, enhanced convective clouds and precipitation have been linked

to thermally driven winds in complex terrain (e.g., Langhans et al., 2013; Cortés-Hernández et al., 2024).

Another reason for the relative scarcity of CPM wind studies is that the response of winds to climate change is highly dependent on future projections of large-scale circulation patterns, which are particularly uncertain across the North Atlantic (e.g., IPCC, 2021; Little et al., 2023). However, some wind systems or wind characteristics are closely related to the terrain and are therefore sufficiently persistent to allow a dedicated study. Here, we examine the added value of a km-scale regional climate model in simulating terrain-related winds in the present climate, as well as the potential added value (i.e., the difference relative to a coarser model) in simulating future change. In addition, we focus on two contrasting wind extremes: very strong winds, which are typically large-scale winds accelerated by terrain, such as downslope windstorms, gap winds or mountain-wave-induced winds, and very weak large-scale winds, which typically result in thermal terrain-generated circulations. Both wind extremes can affect the local population and wildlife in different ways, e.g., through mechanical damage or increased fire risk during strong winds and through stagnant cold air pools or reduced air quality during weak winds.

2   Data and methods

2.1   Model simulations

The CPM simulations were carried out as part of the Nordic Convection Permitting Climate Projections (NorCP) project and are described in detail in Lind et al. (2020, 2023). NorCP is based on the regional climate modeling system HARMONIE-Climate cycle 38 (HCLIM38; Belušić et al., 2020), which consists of two physical configurations: HCLIM38-ALADIN, which is used as a regional climate model (RCM) with a horizontal grid spacing of 12 km (HCLIM12 hereafter), and HCLIM38-AROME, which is used as a CPM with a horizontal grid spacing of 3 km (HCLIM3 hereafter). HCLIM12 is used as an intermediate model to bridge the gap in grid spacing between a global climate model (GCM) and the CPM.

The NorCP climate projections used in this study consist of 20-year time slices in two periods (Table A1), i.e., historical (1986–2005) and end-of-century (2081–2100), downscaling two CMIP5 GCMs, i.e., EC-Earth (Hazeleger et al., 2010, 2012) and GFDL-CM3 (Griffies et al., 2011; Donner et al., 2011). The 21-year-long evaluation simulation (1998–2018) with ERA-Interim (Dee et al., 2011) as the initial and boundary data is used here only for comparison with observations. All simulations were initiated 1 year before the mentioned time slices as the model spin-up. We focus on the RCP8.5 emission scenario because it provides the largest signal-to-noise ratio, especially given the rather short time-slice simulations.

The analyzed model variables are from the near-surface or surface output, with wind speed given at the standard height of 10 m. However, the vertical velocity, which is available only in HCLIM3, is estimated from the model output at constant pressure levels, using the pressure level that is first above the local terrain height at each model grid point and at each output time. Some of these variables are output only every 6 h, thus limiting the range of times in the day available for the analysis of thermal flows.

2.2   Observations, reanalysis and evaluation

Two main sources of historical wind data are used to evaluate the HCLIM model: ERA5 reanalysis data (Hersbach et al., 2020) and in situ wind speed observations from a large number of meteorological observation stations in Sweden (SMHI, 2025). Several studies have assessed the near-surface winds in ERA5 on multiple timescales. These indicate that, in general, ERA5 is able to capture the frequency distributions and average wind speeds, from hourly to seasonal timescales (e.g., Chen et al., 2024; Molina et al., 2021; Fan et al., 2021). However, it has also been shown that ERA5 struggles with representing wind extremes, often overestimating weak winds and underestimating strong winds, and most evidently in areas of complex terrain and in coastal regions (e.g., Belušić Vozila et al., 2024; Potisomporn et al., 2023; Gandoin and Garza, 2024). The wind speed observations from the SMHI observation network are made at 10 m above the ground with a 3 h output frequency, and we have analyzed daily mean values. All station data have undergone quality control and are used in SMHI's operational activities. Stations with more than 30 % missing 3 h time steps have not been considered, leading to a total of 161 stations being used. Figure A1 in Appendix A shows the geographical locations of the stations. Based on their locations, e.g., orography height, these have been categorized into inland flat, coastal and mountain areas. Of the 161 stations, 108 were categorized as inland flat, 32 as coastal and 21 as mountain stations. We use quantile–quantile (Q–Q) plots to compare the distributions of daily mean wind speed values between the two model resolutions, ERA5 and station observations. Each point in a Q–Q plot shows the values of the same quantile from two different datasets, with the final graph providing a clear representation of the relationship between the distributions of the two datasets. Datasets with two identical distributions would follow the identity ($y = x$) line indicated in the corresponding figures below. In the analysis of daily mean wind speeds, we define "weak", "moderate" and "strong" wind speeds as < 5, 5–10 and $> 10\,\mathrm{m\,s^{-1}}$, respectively.

2.3   Selection of strong-wind and weak-wind situations

Strong winds are represented by the 95th percentile of the daily wind maxima, calculated for each time period (i.e., historical and end-of-century) and each grid point separately.

To detect the thermally forced circulation, the analysis is limited to situations with weak synoptic gradients, i.e., weak large-scale winds. For each model grid point, the cases below the 5th percentile of hourly wind speed at 700 hPa are selected and averaged. The final results are tested for robustness to the choice of percentile, and the use of the 2nd percentile gives very similar results. The selection is made separately for winter (DJF) and summer (JJA) and for each climate period (historical and end-of-century). To focus on typical conditions that lead to downslope and upslope winds, and given the limitation of 6 h outputs for some variables, we use the following two representative situations: DJF at 00:00 UTC for stable conditions and JJA at 12:00 UTC for unstable conditions, respectively (Zardi and Whiteman, 2013).

A subdomain covering the southern Scandinavian Mountains is used for the analysis of strong and weak winds, as this is the region with the highest and most complex terrain and this choice limits the otherwise large latitudinal change of the entire Scandinavian Mountains (about 10° of latitude with a length of about 1700 km).

3 Results

3.1 Evaluation of simulated wind speed

The evaluation of the ERA-Interim-forced model results in relation to the station observations and ERA5 is carried out separately for inland stations with predominantly flat terrain, coastal stations and mountain stations (Fig. 1). Both HCLIM12 and HCLIM3 have similar frequency distributions as the station observations for inland stations, and there is no clear added value in the km-scale simulation. Interestingly, ERA5 somewhat overestimates wind speeds for all but the strongest winds in winter. For coastal stations, the models and ERA5 underestimate the strong winds, especially in winter, and the models somewhat underestimate the weak to moderate winds in both seasons, but the overall agreement with the observations is good.

For mountain stations, HCLIM12 and ERA5 considerably underestimate the moderate and strong winds, with the underestimation increasing with wind speed and reaching almost twice smaller values for the strongest winds in winter for ERA5. On the other hand, HCLIM3 agrees very well with the observations, especially in winter. In summer, the wind speeds are slightly underestimated, which is more pronounced for very weak winds. These results clearly show that the km-scale resolution is necessary for modeling strong winds in complex terrain and at the same time imply that the km-scale resolution could be sufficiently high to capture strong mountain winds.

3.2 Assessment of daily mean winds

Focusing on the GCM-forced simulations, we see that the daily mean wind in the historical period is predominantly influenced by large-scale forcing, with the winds being stronger in winter (Fig. 2) than in summer (Fig. 3). The effect of the km-scale resolution is evident in the mountains, where the winds are generally stronger in HCLIM3.

The future change is predominantly governed by the forcing GCM in both seasons. HCLIM simulations forced by EC-Earth (HCLIM12-ECE, HCLIM3-ECE) have smaller changes compared to the GFDL-forced simulations (HCLIM12-GFDL, HCLIM3-GFDL), which show a considerable wind strengthening in the southern part of the domain in winter and a general wind weakening in summer. The differences between HCLIM12 and HCLIM3 downscaling a single GCM are small compared to the differences between HCLIM12 or HCLIM3 forced with different GCMs.

3.3 Strong winds

For the strong winds, Fig. 4 shows that, in the historical period, the HCLIM12 10 m wind speed gradually increases with terrain height and reaches the same values regardless of the forcing GCM in both winter and summer. HCLIM3 is also independent of the GCM forcing in the historical period, but the increase in wind speed with terrain height is much greater than for HCLIM12. For example, at a terrain height of 1500 m, the HCLIM3 wind speed reaches more than $20\,\mathrm{m\,s^{-1}}$ in winter and $14\,\mathrm{m\,s^{-1}}$ in summer, while HCLIM12 reaches only $10\,\mathrm{m\,s^{-1}}$ in winter and $7\,\mathrm{m\,s^{-1}}$ in summer, i.e., twice smaller values. This is consistent with the evaluation results for mountains in Fig. 1 but is even more pronounced here because the focus is on strong wind events.

However, the future change in strong winds is much more affected by the GCM forcing. This is particularly evident for the GFDL forcing in winter, where HCLIM12 and HCLIM3 show very similar future changes at all terrain heights, with wind speed increasing at all levels. In general, it appears that the magnitude of the future changes in both HCLIM12 and HCLIM3 is largely determined by the GCM forcing. However, there are notable differences between the two model resolutions in the dependence on terrain height of the wind speed changes that are likely dependent on model structure and/or grid resolutions. This is particularly evident in summer, where the future change is a general decrease in wind speed at all levels. The percentage decrease is slightly larger for the GFDL forcing compared to the EC-Earth forcing. However, the magnitude of the relative decrease in HCLIM3 becomes consistently larger with terrain height for both GFDL and EC-Earth forcing, while in HCLIM12, the magnitude is quasi-constant with terrain height (EC-Earth forcing) or even increases at higher altitudes (GFDL forcing).
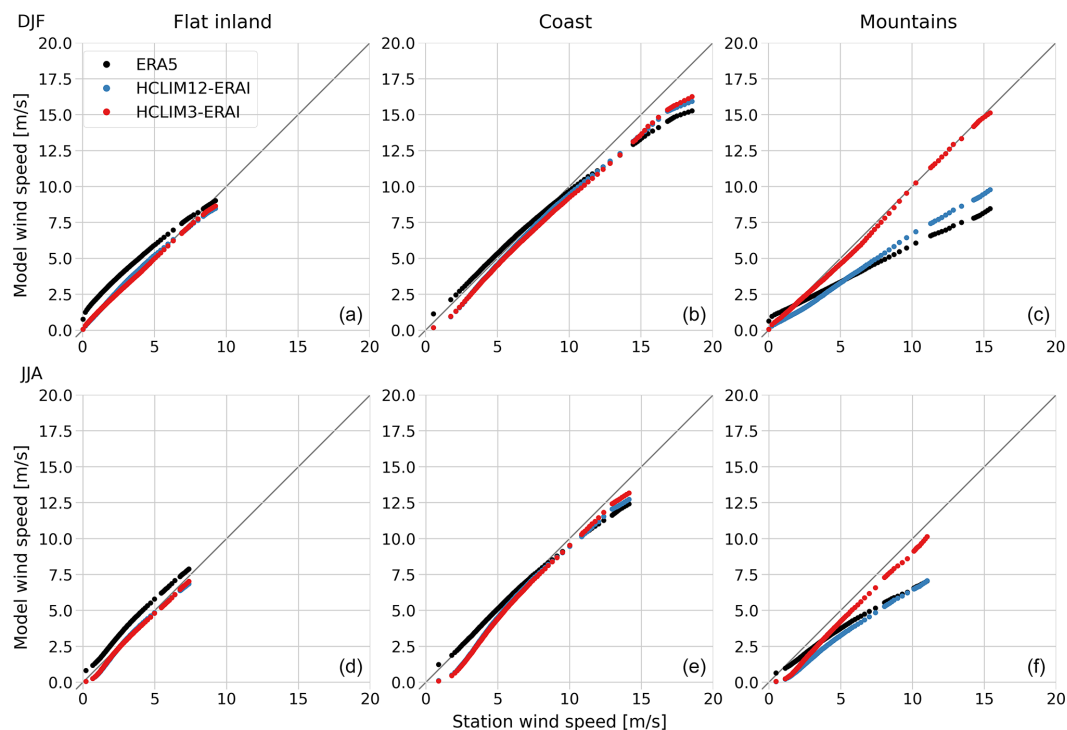
Figure 1. Quantile–quantile plot of daily mean 10 m wind speed in SMHI station data (*x* axis) vs. ERA5 reanalysis and HCLIM evaluation simulations (*y* axis). Shown are DJF **(a–c)** and JJA **(d–f)** for inland stations **(a, d)**, coastal stations **(b, e)** and mountain stations **(c, f)**. The identity (*y* = *x*) line is depicted in gray.
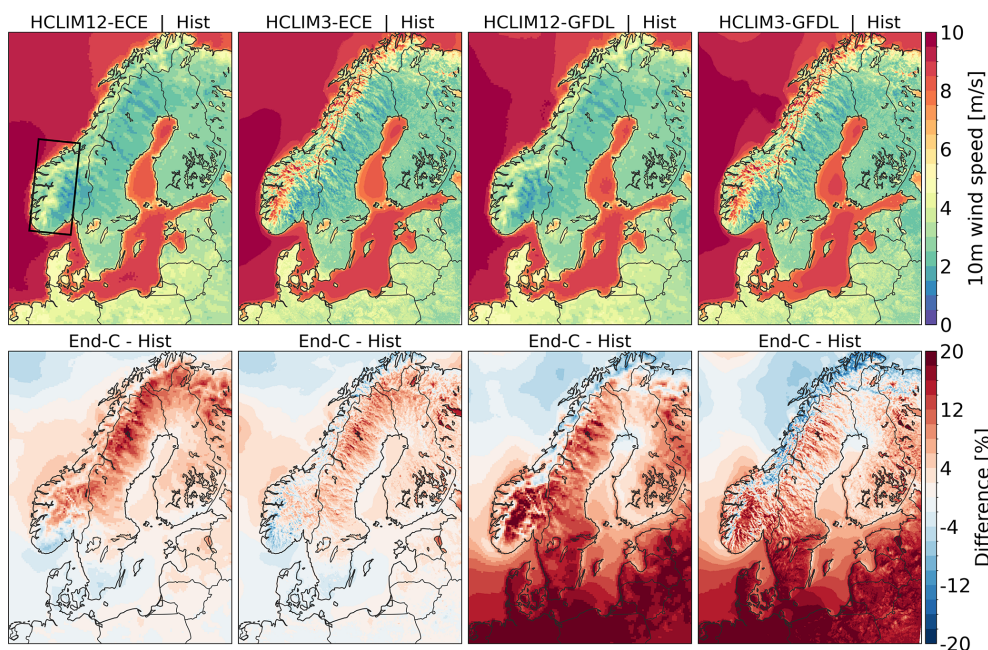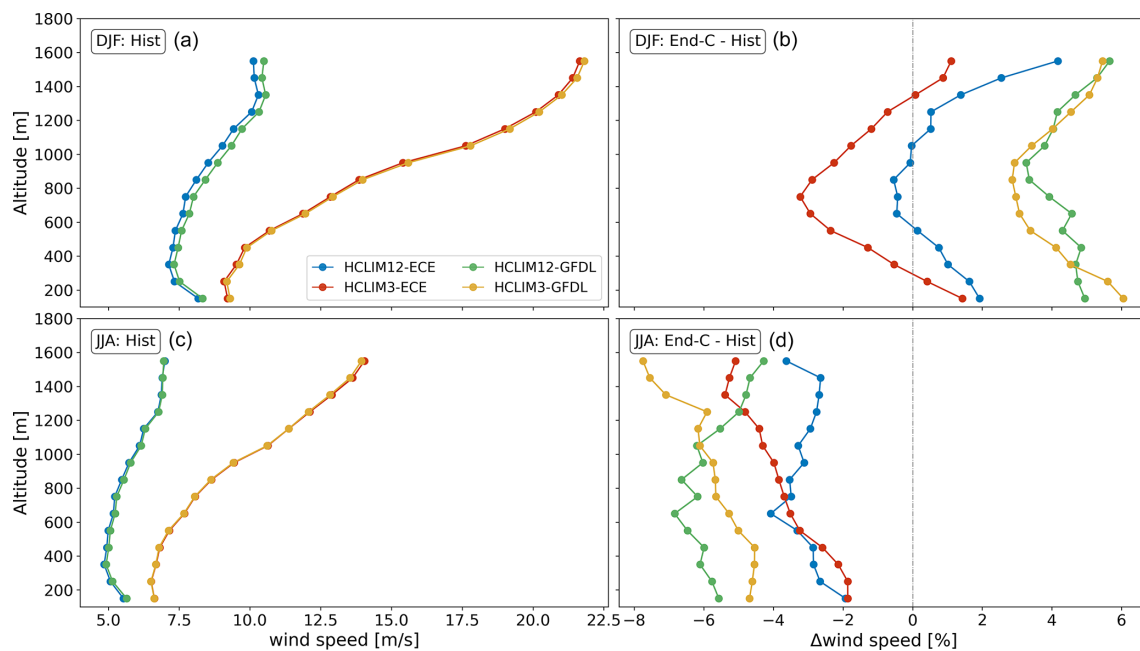

Figure 2. DJF daily mean 10 m wind speed (top panels) and its percentage change by the end of the century (bottom panels) in HCLIM12 and HCLIM3, forced with EC-Earth and GFDL. The black rectangle over southern Norway depicts the domain used for investigating winds over complex terrain.
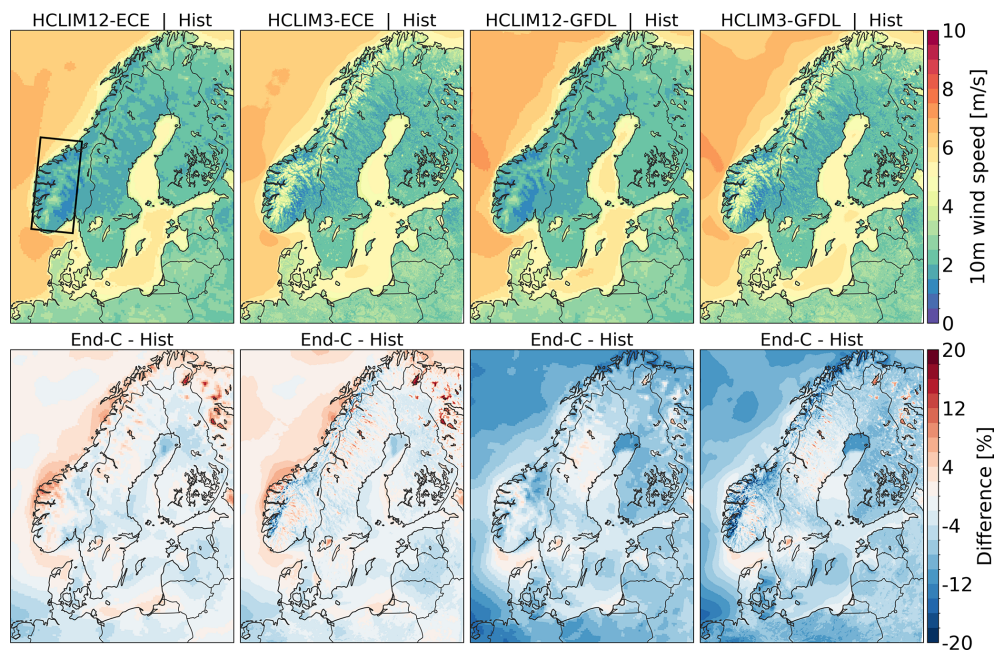
Figure 3. Same as Fig. 2 but for JJA.

Figure 4. The 95th percentile of daily maximum 10 m wind speed as a function of terrain height over the southern Norway subdomain (indicated in Fig. 2) in HCLIM3 and HCLIM12 scenarios for DJF (**a, b**) and JJA (**c, d**). Shown are the wind speeds in the historical period (**a, c**) and the change, in percent, by the end of the century (**b, d**). The data are bin-averaged over 15 vertical bins that are 100 m high.

3.4 Thermal circulations in large-scale weak-wind situations

In large-scale weak wind situations, the thermal circulation systems in the mountains are a superposition of several flows occurring at different scales and typically include mountain-plain circulation, valley flows and slope flows (e.g., Graf et al., 2016). The mountain-plain, and also mountain-ocean in our domain, circulations occur at larger scales that are well reproduced by both HCLIM3 and HCLIM12, so the benefits of km-scale models are limited (e.g., Langhans et al., 2013). Because valley floor widths rarely surpass a few km, neither HCLIM12 nor HCLIM3 can reproduce valley flows accurately (e.g., Wagner et al., 2014; Schmidli et al., 2018). Whereas in the HCLIM12 case the valleys are not resolved at all, there are not enough across-valley grid points in HCLIM3 for accurate depiction of the valley flow (Fig. A2). However, slope flows are present in both model resolutions, albeit additionally smoothened at lower horizontal resolution and hence not accurately representing realistic flows in specific locations. Likewise, insufficient vertical resolution (e.g., Cuxart, 2015; Goger et al., 2022) and inadequate turbulence parameterization (e.g., Grisogono and Belušić, 2008) may hinder accurate representation of slope flows, particularly for stable downslope winds. Because this study addresses a potential added value of km-scale models in the present and future climate, the focus is not on the accurate depiction of thermal circulations at specific locations but on the differences in results between the two model resolutions and on the conceptual comparison of the different results with the theory of such flows. Therefore, we focus the analysis on the differences in slope flows between HCLIM12 and HCLIM3 but acknowledge the existence of other thermal circulations. The thermal slope flows are generated by the terrain slope and buoyancy, with the latter typically expressed as the difference between the air and surface temperatures (e.g., Bintanja et al., 2014). In a nighttime stable boundary layer, the surface is colder than the air next to it due to radiative cooling, resulting in a surface temperature deficit and negative buoyancy, which lead to katabatic (downslope) wind. In a daytime unstable boundary layer, the surface absorbs the incoming solar radiation and is warmer than the air, resulting in positive buoyancy and anabatic (upslope) wind. The presence of snow cover generally lowers the surface temperature compared to the equivalent conditions without snow cover and can cause downslope glacier wind even in daytime conditions (e.g., Van den Broeke, 1997). As stated in Sect. 2, we choose summer daytime and winter nighttime situations as typical representatives of unstable and stable conditions, respectively, for further analysis. Note that we use the term "glacier wind" for katabatic wind caused by snow-covered surfaces in summer daytime situations, even though a glacier need not exist below the snow layer. A more precise name could be katabatic wind caused by perpetual (or summer) snow, but given the strong similarity in characteristics with the true glacier wind, we retain this shorter term.

3.4.1 Unstable conditions

For summer daytime conditions, both HCLIM12 and HCLIM3 in the historical period have similar wind speeds for mountain heights below about 1200 m, gradually decreasing with height (Fig. 5). Above 1200 m, the HCLIM12 wind speed continues to decrease, while the HCLIM3 wind speed rather abruptly starts increasing with height.

The abrupt shift at about 1200 m in HCLIM3 can also be seen in the signal for the future changes. For lower terrain heights, the future change in wind speed is consistently positive in both HCLIM3 and HCLIM12, except for GFDL-forced HCLIM12 below 300 m. For terrain heights above 1200 m, the HCLIM3 future change signal abruptly switches to negative values, while HCLIM12 remains positive. This discrepancy between the RCM and the CPM is examined below.

Note that the exact value of the terrain height at which the change occurs, 1200 m, is determined approximately and varies slightly between the different plots, e.g., it is about 100 m higher for the EC-Earth forcing than for the GFDL forcing. However, as these are composite plots over 20-year periods and many grid points, exact correspondence in the dynamical sense is not to be expected.

The HCLIM3 vertical velocity is positive for terrain heights below 1200 m, confirming the upslope anabatic nature of the summer daytime circulation (Fig. 6). However, the direction of the flow turns to downslope for higher terrain. The direction change is clearly related to the change in snow cover with terrain height, with the direction changing to downslope when the mean snow cover increases to about 30 % (Fig. 6). This suggests that the downslope flow direction is the result of the katabatic glacier wind at those terrain heights, as the presence of snow cover changes the sign of the surface temperature deficit, which is the main forcing for thermal circulations on slopes (e.g., Grisogono and Oerlemans, 2001). This is seen from the vertical profiles of the temperature deficit (Fig. 7), which has nearly constant negative values (positive buoyancy) below 1200 m, above which it rapidly increases and crosses zero between 1400 and 1600 m, depending on the forcing GCM (the zero-crossing for the EC-Earth forcing is not seen in the figure because the vertical axis is clipped below 1600 m due to too few grid points in HCLIM12 aloft). HCLIM12 has a similar vertical profile of the temperature deficit, but the increase above 1200 m is weaker.

Vertical velocity is not available for HCLIM12, but horizontal wind divergence can be used to detect differences in flow regimes between HCLIM12 and HCLIM3. The horizontal wind divergence in HCLIM3 (Fig. 8), which indicates a developed downslope flow over at least two grid points on a slope, occurs above 1400 m, where the snow cover ex-
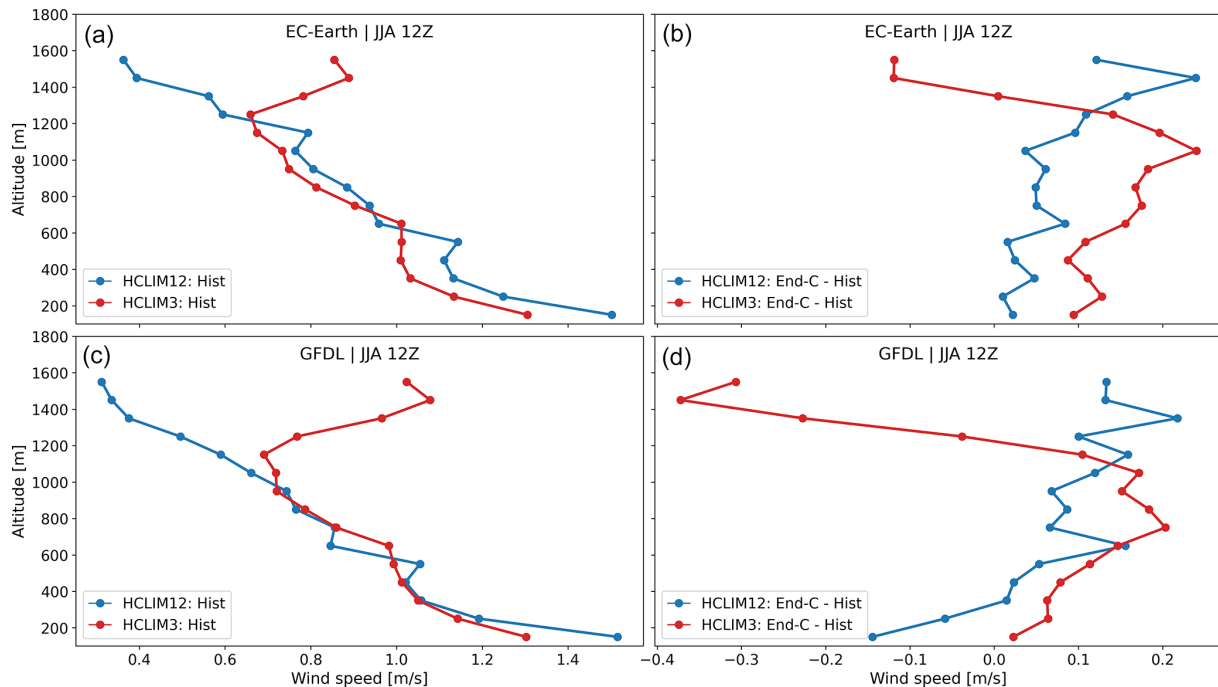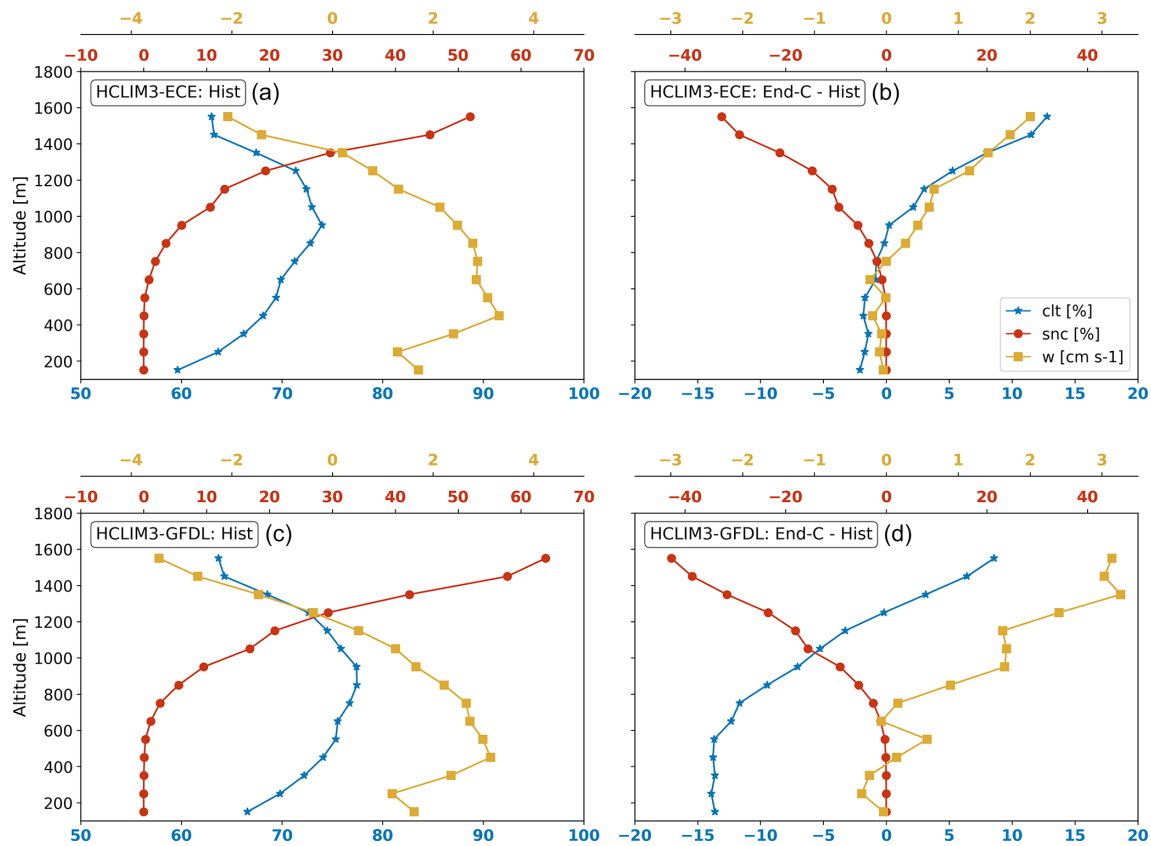
Figure 5. HCLIM12 and HCLIM3 simulated JJA 12:00 UTC wind speed as a function of terrain height over the southern Norway subdomain (indicated in Fig. 2) for large-scale weak-wind conditions (see text for explanation). Shown are the historical period **(a, c)** and the changes by the end of the century **(b, d)** in HCLIM3-ECE **(a, b)** and HCLIM3-GFDL **(c, d)**. The data are bin-averaged over 15 vertical bins that are 100 m high.

ceeds 40 %. This has important implications for understanding the differences between the RCM and the CPM. Both HCLIM12 and HCLIM3 have grid points with snow cover above 40 %. However, analysis of the spatial patterns (e.g., Fig. A2) reveals that HCLIM12, unlike HCLIM3, predominantly has fewer than two such neighboring grid points on a single slope, which seems to prevent the development of divergence and consequently katabatic flow even at high terrain altitudes, i.e., near mountain tops. This also prevents HCLIM12 from reaching a bin-averaged positive temperature deficit in high terrain (Fig. 7). Consequently, HCLIM12 has an upslope flow at all levels that gradually weakens with height (Fig. 5), i.e., there is weak convergence at all levels (Fig. 8). In HCLIM3, the upslope flow below 1200 m meets the downslope glacier flow from above, and a stronger convergence zone develops, reaching its maximum at terrain heights between 1000 and 1200 m (Fig. 8).

The existence of the convergence zone in HCLIM3 has an impact on cloud cover. HCLIM3 cloud cover gradually increases with height, reaching the maximum of about 80 % at about 1000 m, exactly at the height of maximum convergence, and decreases in the divergence regions above (Fig. 6). HCLIM12 has a gradual increase in cloud cover with height, without a clear maximum and in line with the convergence at all heights (Fig. A3).

With future warming, the HCLIM3 temperature deficit decreases, indicating further destabilization of the surface layer

(Fig. 7). The destabilization generally increases with terrain height up to about 1300 m. HCLIM12 has a similar future change profile, except that there is weak stabilization for the lower terrain heights, especially for the GFDL forcing. The future wind speed change is generally positive and increases approximately linearly with height (Fig. 5), which is consistent with the increase in destabilization with height. There are two exceptions to the linear wind speed increase with height: the wind speed decrease in the GFDL-forced HCLIM12 below 300 m, which is consistent with the low-level stabilization, and the abrupt change in HCLIM3 occurring between 1000 and 1200 m, resulting in wind speed decrease aloft. For the latter, the decrease in summer snow cover above 1200 m (Fig. 6) reduces the spatial extent and strength of the downslope flow in HCLIM3. This is evident from the combined positive change in vertical velocity (Fig. 6) and the decrease in wind speed (Fig. 5), which indicates the weakening of the downslope flow and its transition to higher terrain, together with the formation of a weaker upslope flow below. As the divergence zone also weakens and moves to higher terrain (Fig. 8), the HCLIM3 cloud cover increases above 1200 m (Fig. 6). The changes in cloud cover in HCLIM12 are much smaller, despite the comparable snowmelt (Fig. A3). This is a further indication that the dynamics of the glacier wind was not reproduced by HCLIM12 in the present climate, and hence the future warming affects the mountain circulation much less. Namely, the future warming and snowmelt in

Figure 6. HCLIM3 simulated JJA 12:00 UTC cloud cover (clt; blue line/stars), snow cover (snc; red line/circles) and vertical wind speed (w; yellow line/squares) as a function of terrain height over the southern Norway subdomain (indicated in Fig. 2) for large-scale weak-wind conditions (see text for explanation). Shown are the historical period **(a, c)** and the changes by the end of the century in RCP8.5 **(b, d)** in HCLIM3-ECE **(a, b)** and HCLIM3-GFDL **(c, d)**. The data are bin-averaged over 15 vertical bins that are 100 m high.

HCLIM12 result in the upslope wind strengthening at all levels, but without changing the nature or direction of the flow.

3.4.2 Stable conditions

The winter nighttime situation is simpler. The vertical velocity is negative at all terrain heights (Fig. A4), so the flow is downslope, as expected in stable conditions. There is a difference between the RCM and the CPM: the wind speed gradually decreases with terrain height in the RCM, whereas it increases quite strongly in the CPM (Fig. 9). The latter is partly caused by much stronger winds in a few grid points in the CPM with very steep terrain, the proportion of which increases with height. In other words, this strong increase does not show up when the median is used instead of the mean to calculate the vertical bins, at least below 1000 m. This behavior is almost the same regardless of the forcing GCM. With future warming and the associated snowmelt, the surface is destabilized, leading to weaker winds at all heights. The relative wind weakening is similar at all terrain heights, ranging between 10 % and 20 %.

4 Discussion and conclusion

The benefits of km-scale modeling for winds depend on the complexity of the terrain, the nature of wind and the type of signal that is addressed, the latter being either the behavior in a given climate period or the change between different climates. The expected general conclusion is that the greatest added value of higher-resolution modeling is found in complex mountainous terrain, which is a direct consequence of the better representation of the terrain. However, the evaluation also shows that the km-scale resolution might be sufficiently high to capture strong winds in complex terrain, at least when considering the setup of the available observation stations. The latter is, of course, highly dependent on the local terrain, and in many locations with complex terrain at small scales, sub-km resolution is advantageous or even crucial (e.g., Wang et al., 2013; Goger and Dipankar, 2024).

All wind types show benefits of km-scale modeling in complex terrain, but in different ways. For the mean and strong winds, the differences in wind speed can be very large, especially in higher terrain, reaching twice stronger winds in the km-scale model than in the RCM. In the case of weak,
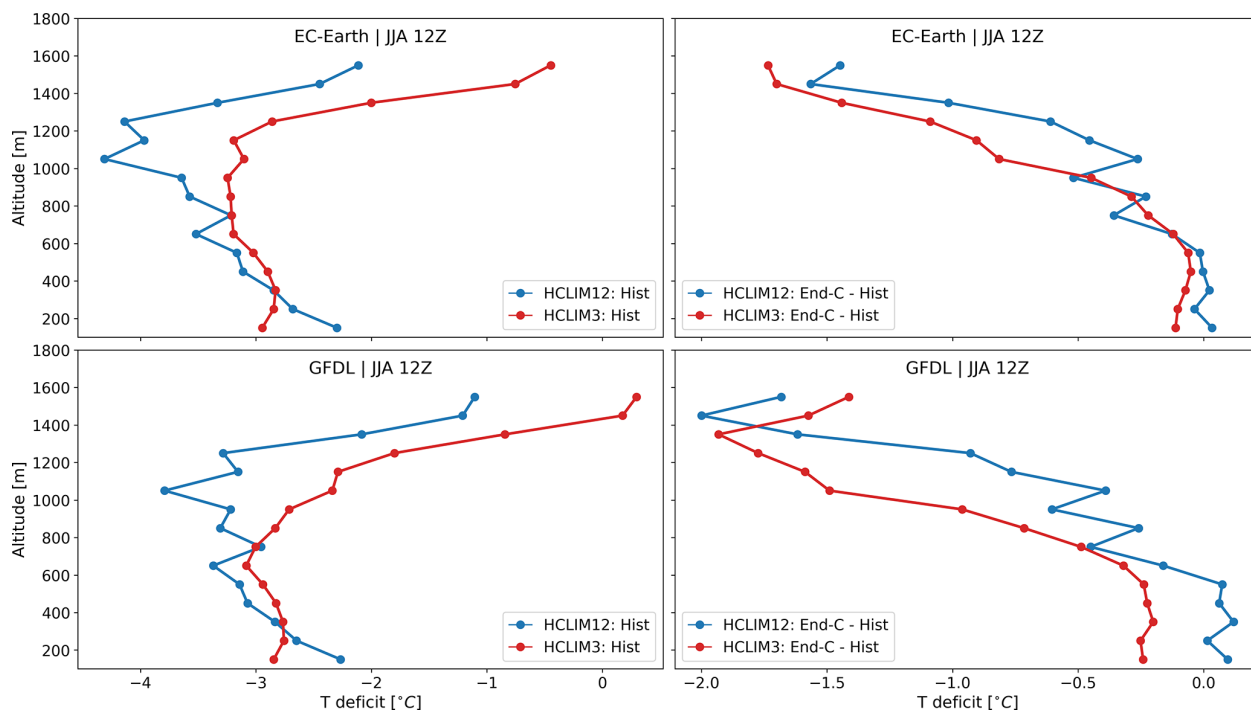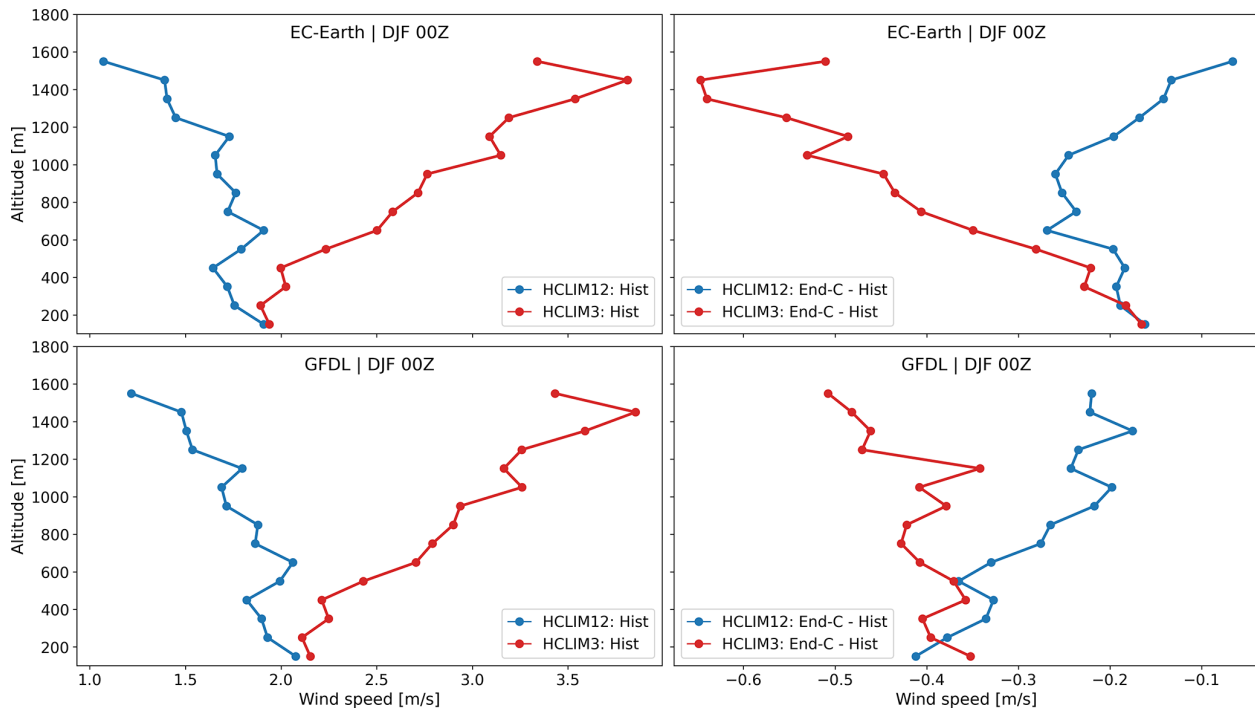
Figure 7. Same as Fig. 5 but showing surface temperature deficit. The surface temperature deficit is defined as the difference between the temperature at the lowest model level (approximately 12 m above the terrain) and the surface radiation temperature.
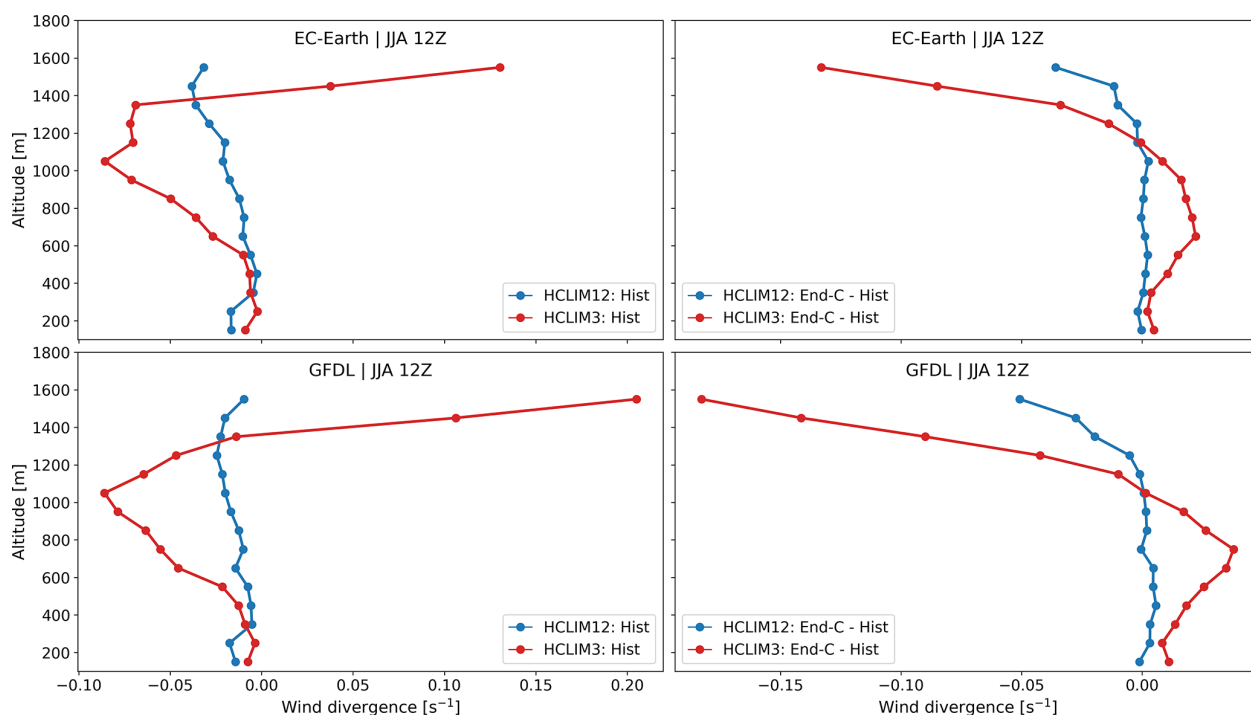
Figure 8. Same as Fig. 5 but showing divergence.

Figure 9. Same as Fig. 5 but for DJF at 00:00 UTC.

thermally generated winds, in unstable summer daytime conditions, the km-scale model can reproduce the downslope glacier wind and the resulting divergence in high terrain, as well as the convergence in and around the frontal zone where the downslope glacier and upslope daytime winds meet. This affects the vertical distribution of cloud cover, which reaches its maximum in the convergence zone, consistent with the glacier fronts in the Himalayas (Lin et al., 2021). The RCM fails to reproduce the glacier wind. In stable winter nighttime conditions, both models reproduce the downslope katabatic flow, albeit with different terrain dependence: the strengthening of the wind with terrain height is evident only in the CPM.

The future change signal for the mean and strong winds is mostly influenced by the GCM forcing in that the GCM forcing determines the magnitude of the wind change, while the vertical dependence of the change signal is resolution-dependent. For weak, thermally generated winds under unstable conditions, future warming with melting snow affects the RCM and CPM differently. Because the km-scale model reproduces the glacier wind, the future warming and the associated snowmelt cause the glacier wind to cease or decrease, weakening the convergence zone and shifting it to higher terrain. On the other hand, because there is no downslope glacier wind in the RCM in the historical period, the snowmelt in the RCM leads to a strengthening of the already existing upslope flow. Under stable conditions, the future wind weakening is a consequence of destabilization due to warming and snowmelt and is similar in both models. Both

the general strengthening of the daytime upslope wind and the weakening of the nighttime downslope wind with future warming are consistent with the results obtained for the Rocky Mountains in the USA (Letcher and Minder, 2017).

For thermal circulations, the future change is only weakly dependent on GCM forcing, primarily due to the different GCM warming levels rather than large-scale circulation changes. Because future surface warming is a much less uncertain result compared to circulation changes, it may be possible to determine the fate of local thermal circulations in the future climate with comparatively high confidence.

Appendix A

Table A1. Overview of simulations from the NorCP experiment (Lind et al., 2020, 2023) analyzed in this study.

Simulation	Period	Boundary data
Evaluation	1998–2018	ERA-Interim
Historical	1986–2005	EC-Earth, GFDL
End-of-century	2081–2100	EC-Earth, GFDL – RCP 8.5
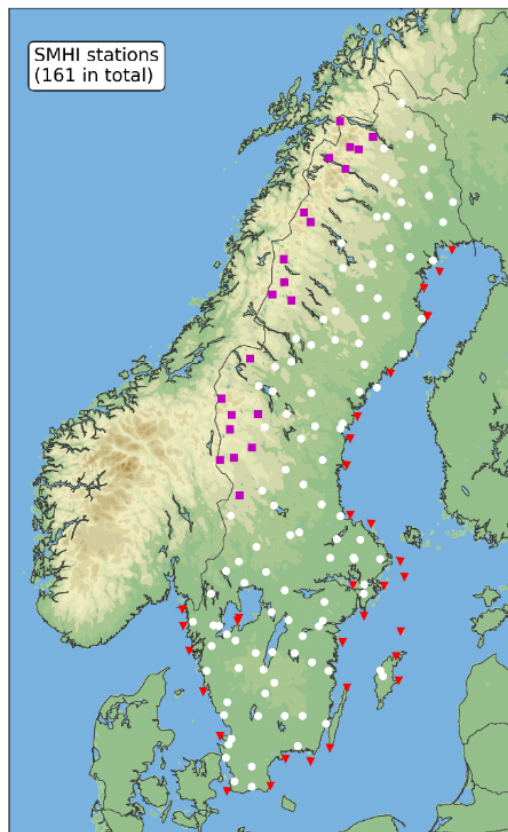
Figure A1. The spatial distribution of the SMHI stations used in the analysis of daily mean wind speed. A total of 161 stations were used in the study and categorized into inland flat (white circles), coastal (red triangles) and mountain (purple squares) stations.
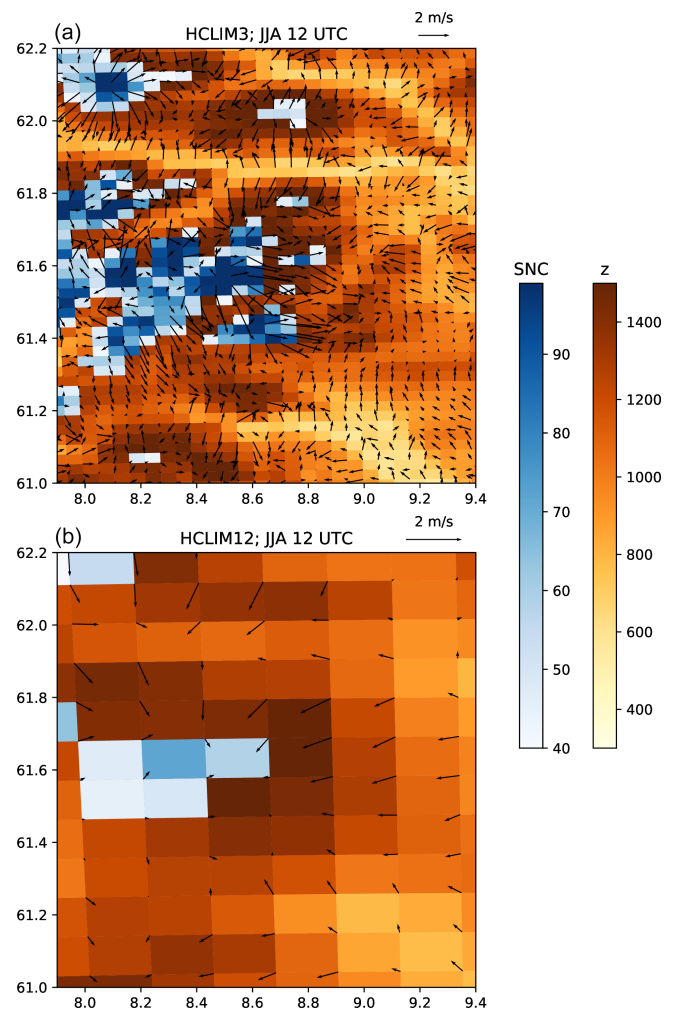
Figure A2. An enlarged view of the central part of the southern Scandinavian Mountains domain for JJA at 12:00 UTC, showing terrain height, snow cover above 40 % and wind vectors for HCLIM3 (a) and HCLIM12 (b). Shown are the composite values over the historical period for the synoptically weak-wind days, as defined in the paper.
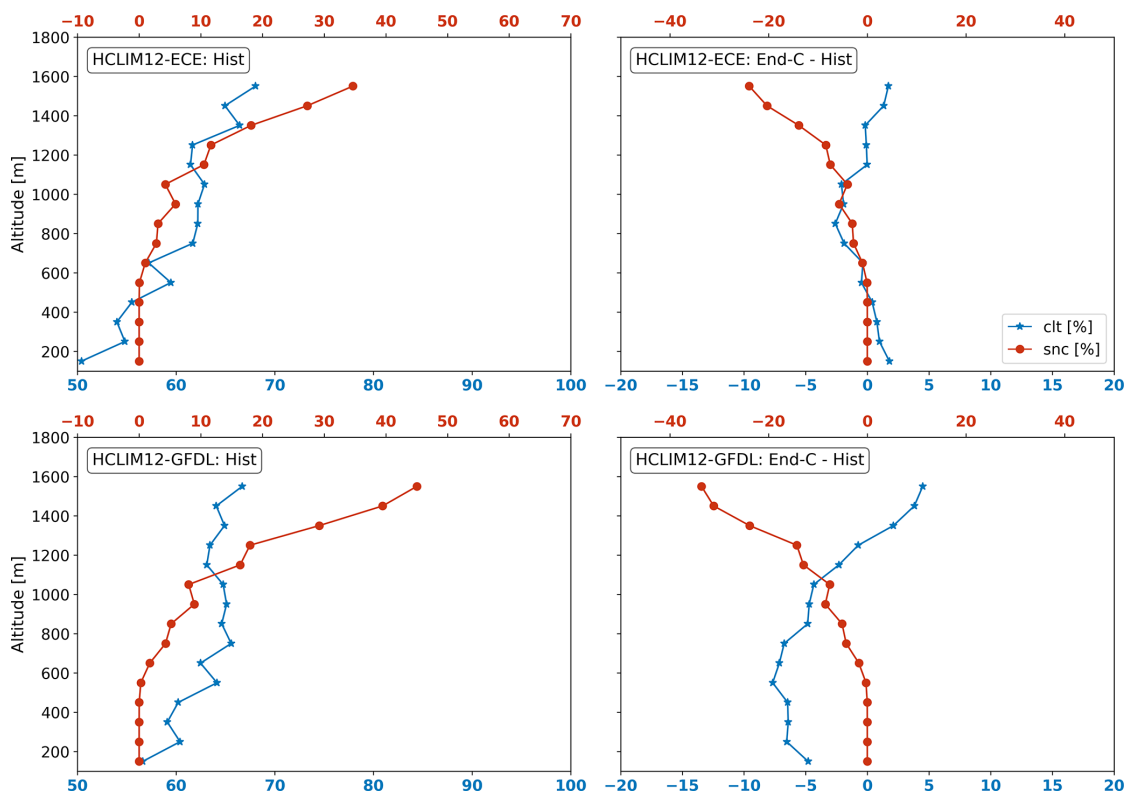
Figure A3. Same as Fig. 6 but showing HCLIM12 cloud cover and snow cover.

Figure A4. Same as Fig. 6 but showing DJF at 00:00 UTC.

References

Ban, N., Caillaud, C., Coppola, E., Pichelli, E., Sobolowski, S., Adinolfi, M., Ahrens, B., Alias, A., Anders, I., Bastin, S., Belušić, D., Berthou, S., Brisson, E., Cardoso, R. M., Chan, S. C., Christensen, O. B., Fernández, J., Fita, L., Frisius, T., Gašparac, G., Giorgi, F., Goergen, K., Haugen, J. E., Hodnebrog, Ø., Kartsios, S., Katragkou, E., Kendon, E. J., Keuler, K., Lavin-Gullon, A., Lenderink, G., Leutwyler, D., Lorenz, T., Maraun, D., Mercogliano, P., Milovac, J., Panitz, H.-J., Raffa, M., Remedio, A. R., Schär, C., Soares, P. M. M., Srnec, L., Steensen, B. M., Stocchi, P., Tölle, M. H., Truhetz, H., Vergara-Temprado, J., de Vries, H., Warrach-Sagi, K., Wulfmeyer, V., and Zander, M. J.: The first multi-model ensemble of regional climate simulations at kilometer-scale resolution, part I: evaluation of precipitation, Clim. Dynam., 57, 275–302, https://doi.org/10.1007/s00382-021-05708-w, 2021.

Belušić, A., Prtenjak, M. T., Güttler, I., Ban, N., Leutwyler, D., and Schär, C.: Near-surface wind variability over the broader Adriatic region: insights from an ensemble of regional climate models, Clim. Dynam., 50, 4455–4480, https://doi.org/10.1007/s00382-017-3885-5, 2018.

Belušić, D., de Vries, H., Dobler, A., Landgren, O., Lind, P., Lindstedt, D., Pedersen, R. A., Sánchez-Perrino, J. C., Toivonen, E., van Ulft, B., Wang, F., Andrae, U., Batrak, Y., Kjellström, E., Lenderink, G., Nikulin, G., Pietikäinen, J.-P., Rodríguez-Camino, E., Samuelsson, P., van Meijgaard, E., and Wu, M.: HCLIM38: a flexible regional climate model applicable for different climate zones from coarse to convection-permitting scales, Geosci. Model Dev., 13, 1311–1333, https://doi.org/10.5194/gmd-13-1311-2020, 2020.

Belušić Vozila, A., Belušić, D., Telišman Prtenjak, M., Güttler, I., Bastin, S., Brisson, E., Demory, M.-E., Dobler, A., Feldmann, H., Hodnebrog, Ø., Kartsios, S., Keuler, K., Lorenz, T., Milovac, J., Pichelli, E., Raffa, M., Soares, P. M. M., Tölle, M. H., Truhetz, H., de Vries, H., and Warrach-Sagi, K.: Evaluation of the near-surface wind field over the Adriatic region: local wind characteristics in the convection-permitting model ensemble, Clim. Dynam., 62, 4617–4634, https://doi.org/10.1007/s00382-023-06703-z, 2024.

Berthou, S., Kendon, E. J., Chan, S. C., Ban, N., Leutwyler, D., Schär, C., and Fosser, G.: Pan-European climate at convection-permitting scale: a model intercomparison study, Clim. Dynam., 55, 35–59, https://doi.org/10.1007/s00382-018-4114-6, 2020.

Bintanja, R., Severijns, C., Haarsma, R., and Hazeleger, W.: The future of Antarctica's surface winds simulated by a high-resolution global climate model: 2. Drivers of 21st century changes, J. Geophys. Res.-Atmos., 119, 7160–7178, https://doi.org/10.1002/2013JD020848, 2014.

Chen, T.-C., Collet, F., and Di Luca, A.: Evaluation of ERA5 precipitation and 10 m wind speed associated with extratropical cyclones using station data over North America, Int. J. Climatol., 44, 729–747, https://doi.org/10.1002/joc.8339, 2024.

Cholette, M., Laprise, R., and Thériault, J. M.: Perspectives for Very High-Resolution Climate Simulations with Nested Models: Illustration of Potential in Simulating St. Lawrence River Valley Channelling Winds with the Fifth-Generation Canadian Regional Climate Model, Climate, 3, 283–307, https://doi.org/10.3390/cli3020283, 2015.

Cortés-Hernández, V. E., Caillaud, C., Bellon, G., Brisson, E., Alias, A., and Lucas-Picher, P.: Evaluation of the convection permitting regional climate model CNRM-AROME on the orographically complex island of Corsica, Clim. Dynam., 62, 4673–4696, https://doi.org/10.1007/s00382-024-07232-z, 2024.

Cuxart, J.: When Can a High-Resolution Simulation Over Complex Terrain be Called LES?, Front. Earth Sci., 3, 87, https://doi.org/10.3389/feart.2015.00087, 2015.

Dee, D. P., Uppala, S. M., Simmons, A. J., Berrisford, P., Poli, P., Kobayashi, S., Andrae, U., Balmaseda, M. A., Balsamo, G., Bauer, P., Bechtold, P., Beljaars, A. C. M., van de Berg, L., Bidlot, J., Bormann, N., Delsol, C., Dragani, R., Fuentes, M., Geer, A. J., Haimberger, L., Healy, S. B., Hersbach, H., Hólm, E. V., Isaksen, L., Kållberg, P., Köhler, M., Matricardi, M., McNally, A. P., Monge-Sanz, B. M., Morcrette, J.-J., Park, B.-K., Peubey, C., de Rosnay, P., Tavolato, C., Thépaut, J.-N., and Vitart, F.: The ERA-Interim reanalysis: configuration and performance of the data assimilation system, Q. J. Roy. Meteor. Soc., 137, 553–597, https://doi.org/10.1002/qj.828, 2011.

Donner, L. J., Wyman, B. L., Hemler, R. S., Horowitz, L. W., Ming, Y., Zhao, M., Golaz, J.-C., Ginoux, P., Lin, S.-J., Schwarzkopf, M. D., Austin, J., Alaka, G., Cooke, W. F., Delworth, T. L., Freidenreich, S. M., Gordon, C. T., Griffies, S. M., Held, I. M., Hurlin, W. J., Klein, S. A., Knutson, T. R., Langenhorst, A. R., Lee, H.-C., Lin, Y., Magi, B. I., Malyshev, S. L., Milly, P. C. D., Naik, V., Nath, M. J., Pincus, R., Ploshay, J. J., Ramaswamy, V., Seman, C. J., Shevliakova, E., Sirutis, J. J., Stern, W. F., Stouffer, R. J., Wilson, R. J., Winton, M., Wittenberg, A. T., and Zeng, F.: The Dynamical Core, Physical Parameterizations, and Basic Simulation Characteristics of the Atmospheric Component AM3 of the GFDL Global Coupled Model CM3, J. Climate, 24, 3484–3519, https://doi.org/10.1175/2011JCLI3955.1, 2011.

Fan, W., Liu, Y., Chappell, A., Dong, L., Xu, R., Ekström, M., Fu, T.-M., and Zeng, Z.: Evaluation of Global Reanalysis Land Surface Wind Speed Trends to Support Wind Energy Development Using In Situ Observations, J. Appl. Meteorol. Clim., 60, 33–50, https://doi.org/10.1175/JAMC-D-20-0037.1, 2021.

Gandoin, R. and Garza, J.: Underestimation of strong wind speeds offshore in ERA5: evidence, discussion and correction, Wind Energ. Sci., 9, 1727–1745, https://doi.org/10.5194/wes-9-1727-2024, 2024.

Goger, B. and Dipankar, A.: The impact of mesh size, turbulence parameterization, and land-surface-exchange scheme on simulations of the mountain boundary layer in the hectometric range, Q. J. Roy. Meteor. Soc., 150, 3853–3873, https://doi.org/10.1002/qj.4799, 2024.

Goger, B., Stiperski, I., Nicholson, L., and Sauter, T.: Large-eddy simulations of the atmospheric boundary layer over an Alpine glacier: Impact of synoptic flow direction and governing processes, Q. J. Roy. Meteor. Soc., 148, 1319–1343, https://doi.org/10.1002/qj.4263, 2022.

Graf, M., Kossmann, M., Trusilova, K., and Mühlbacher, G.: Identification and Climatology of Alpine Pumping from a Regional Climate Simulation, Front. Earth Sci., 4, 5, https://doi.org/10.3389/feart.2016.00005, 2016.

Griffies, S. M., Winton, M., Donner, L. J., Horowitz, L. W., Downes, S. M., Farneti, R., Gnanadesikan, A., Hurlin, W. J., Lee, H.-C., Liang, Z., Palter, J. B., Samuels, B. L., Wittenberg, A. T., Wyman, B. L., Yin, J., and Zadeh, N.: The GFDL CM3 Coupled Climate Model: Characteristics of the Ocean and Sea Ice Simulations, J. Climate, 24, 3520–3544, https://doi.org/10.1175/2011JCLI3964.1, 2011.

Grisogono, B. and Belušić, D.: Improving mixing length-scale for stable boundary layers, Q. J. Roy. Meteor. Soc., 134, 2185–2192, https://doi.org/10.1002/qj.347, 2008.

Grisogono, B. and Oerlemans, J.: Katabatic Flow: Analytic Solution for Gradually Varying Eddy Diffusivities, J. Atmos. Sci., 58, 3349–3354, https://doi.org/10.1175/1520-0469(2001)058<3349:KFASFG>2.0.CO;2, 2001.

Hazeleger, W., Severijns, C., Semmler, T., Ştefănescu, S., Yang, S., Wang, X., Wyser, K., Dutra, E., Baldasano, J. M., Bintanja, R., Bougeault, P., Caballero, R., Ekman, A. M. L., Christensen, J. H., van den Hurk, B., Jimenez, P., Jones, C., Kållberg, P., Koenigk, T., McGrath, R., Miranda, P., van Noije, T., Palmer, T., Parodi, J. A., Schmith, T., Selten, F., Storelvmo, T., Sterl, A., Tapamo, H., Vancoppenolle, M., Viterbo, P., and Willén, U.: EC-Earth: A Seamless Earth-System Prediction Approach in Action, B. Am. Meteorol. Soc., 91, 1357–1364, https://doi.org/10.1175/2010BAMS2877.1, 2010.

Hazeleger, W., Wang, X., Severijns, C., Ştefănescu, S., Bintanja, R., Sterl, A., Wyser, K., Semmler, T., Yang, S., van den Hurk, B., van Noije, T., van der Linden, E., and van der Wiel, K.: EC-Earth V2.2: description and validation of a new seamless earth system prediction model, Clim. Dynam., 39, 2611–2629, https://doi.org/10.1007/s00382-011-1228-5, 2012.

Hersbach, H., Bell, B., Berrisford, P., Hirahara, S., Horányi, A., Muñoz-Sabater, J., Nicolas, J., Peubey, C., Radu, R., Schepers, D., Simmons, A., Soci, C., Abdalla, S., Abellan, X., Balsamo, G., Bechtold, P., Biavati, G., Bidlot, J., Bonavita, M., De Chiara, G., Dahlgren, P., Dee, D., Diamantakis, M., Dragani, R., Flemming, J., Forbes, R., Fuentes, M., Geer, A., Haimberger, L., Healy, S., Hogan, R. J., Hólm, E., Janisková, M., Keeley, S., Laloyaux, P., Lopez, P., Lupu, C., Radnoti, G., de Rosnay, P., Rozum, I., Vamborg, F., Villaume, S., and Thépaut, J.-N.: The ERA5 global reanalysis, Q. J. Roy. Meteor. Soc., 146, 1999–2049, https://doi.org/10.1002/qj.3803, 2020.

Hersbach, H., Bell, B., Berrisford, P., Biavati, G., Horányi, A., Muñoz Sabater, J., Nicolas, J., Peubey, C., Radu, R., Rozum, I., Schepers, D., Simmons, A., Soci, C., Dee, D., and Thépaut, J.-N.: ERA5 hourly data on single levels from 1940 to present, Copernicus Climate Change Service (C3S) Climate Data Store (CDS) [data set], https://doi.org/10.24381/cds.adbb2d47, 2023.

IPCC: Summary for Policymakers, in: Climate Change 2021: The Physical Science Basis. Contribution of Working Group I to the Sixth Assessment Report of the Intergovernmental Panel on Climate Change, edited by: Masson-Delmotte, V., Zhai, P., Pirani, A., Connors, S. L., Péan, C., Berger, S., Caud, N., Chen, Y., Goldfarb, L., Gomis, M. I., Huang, M., Leitzell, K., Lonnoy, E., Matthews, J. B. R., Maycock, T. K., Waterfield, T., Yelekçi, O., Yu, R., and Zhou, B., Cambridge University Press, Cambridge, United Kingdom and New York, NY, USA, 3–32, https://doi.org/10.1017/9781009157896.001, 2021.

Langhans, W., Schmidli, J., Fuhrer, O., Bieri, S., and Schär, C.: Long-Term Simulations of Thermally Driven Flows and Orographic Convection at Convection-Parameterizing and Cloud-Resolving Resolutions, J. Appl. Meteorol. Clim., 52, 1490–1510, https://doi.org/10.1175/JAMC-D-12-0167.1, 2013.

Letcher, T. W. and Minder, J. R.: The Simulated Response of Diurnal Mountain Winds to Regionally Enhanced Warming Caused by the Snow Albedo Feedback, J. Atmos. Sci., 74, 49–67, https://doi.org/10.1175/JAS-D-16-0158.1, 2017.

Lin, C., Yang, K., Chen, D., Guyennon, N., Balestrini, R., Yang, X., Acharya, S., Ou, T., Yao, T., Tartari, G., and Salerno, F.: Summer afternoon precipitation associated with wind convergence near the Himalayan glacier fronts, Atmos. Res., 259, 105658–105658, https://doi.org/10.1016/j.atmosres.2021.105658, 2021.

Lind, P. and Belušić, D.: Data and codes used in "Benefits of km-scale climate modeling for winds in complex terrain: strong versus weak winds", Zenodo [data set], https://doi.org/10.5281/zenodo.15000594, 2025.

Lind, P., Belušić, D., Christensen, O. B., Dobler, A., Kjellström, E., Landgren, O., Lindstedt, D., Matte, D., Pedersen, R. A., Toivonen, E., and Wang, F.: Benefits and added value of convection-permitting climate modeling over Fenno-Scandinavia, Clim. Dynam., 55, 1893–1912, https://doi.org/10.1007/s00382-020-05359-3, 2020.

Lind, P., Belušić, D., Médus, E., Dobler, A., Pedersen, R. A., Wang, F., Matte, D., Kjellström, E., Landgren, O., Lindstedt, D., Christensen, O. B., and Christensen, J. H.: Climate change information over Fenno-Scandinavia produced with a convection-permitting climate model, Clim. Dynam., 61, 519–541, https://doi.org/10.1007/s00382-022-06589-3, 2023.

Little, A. S., Priestley, M. D. K., and Catto, J. L.: Future increased risk from extratropical windstorms in northern Europe, Nat. Commun., 14, 4434–4434, https://doi.org/10.1038/s41467-023-40102-6, 2023.

Lucas-Picher, P., Argüeso, D., Brisson, E., Tramblay, Y., Berg, P., Lemonsu, A., Kotlarski, S., and Caillaud, C.: Convection-permitting modeling with regional climate models: Latest developments and next steps, WIREs Clim. Change, 12, e731–e731, https://doi.org/10.1002/wcc.731, 2021.

Molina, M. O., Gutiérrez, C., and Sánchez, E.: Comparison of ERA5 surface wind speed climatologies over Europe with observations from the HadISD dataset, Int. J. Climatol., 41, 4864–4878, https://doi.org/10.1002/joc.7103, 2021.

Molina, M. O., Careto, J. M., Gutiérrez, C., Sánchez, E., Goergen, K., Sobolowski, S., Coppola, E., Pichelli, E., Ban, N., Belušić, D., Short, C., Caillaud, C., Dobler, A., Hodnebrog, Ø., Kartsios, S., Lenderink, G., de Vries, H., Göktürk, O., Milovac, J., Feldmann, H., Truhetz, H., Demory, M. E., Warrach-Sagi, K., Keuler, K., Adinolfi, M., Raffa, M., Tölle, M., Sieck, K., Bastin, S., and Soares, P. M. M.: The added value of simulated near-surface wind speed over the Alps from a km-scale multimodel ensemble, Clim. Dynam., 62, 4697–4715, https://doi.org/10.1007/s00382-024-07257-4, 2024.

Potisomporn, P., Adcock, T. A. A., and Vogel, C. R.: Evaluating ERA5 reanalysis predictions of low wind speed events around the UK, Energy Reports, 10, 4781–4790, https://doi.org/10.1016/j.egyr.2023.11.035, 2023.

Prein, A. F., Langhans, W., Fosser, G., Ferrone, A., Ban, N., Goergen, K., Keller, M., Tölle, M., Gutjahr, O., Feser, F., Brisson, E., Kollet, S., Schmidli, J., van Lipzig, N. P. M., and Leung, R.: A review on regional convection-permitting climate modeling: Demonstrations, prospects, and challenges, Rev. Geophys., 53, 323–361, https://doi.org/10.1002/2014RG000475, 2015.

Schmidli, J., Böing, S., and Fuhrer, O.: Accuracy of Simulated Diurnal Valley Winds in the Swiss Alps: Influence of Grid Resolution, Topography Filtering, and Land Surface Datasets, Atmosphere, 9, 196, https://doi.org/10.3390/atmos9050196, 2018.

SMHI: Average wind, gust and wind direction, SMHI [data set], https://www.smhi.se/data/temperatur-och-vind/vind/wind (last access: 21 August 2025), 2025.

The HARMONIE Climate community: NorCP HCLIM 12km ERA-Interim data, NIRD RDA [data set], https://doi.org/10.11582/2025.00046, 2025a.

The HARMONIE Climate community: NorCP HCLIM 3km ERA-Interim data, NIRD RDA [data set], https://doi.org/10.11582/2025.00064, 2025b.

Van den Broeke, M. R.: Structure and diurnal variation of the atmospheric boundary layer over a mid-latitude glacier in summer, Bound.-Lay. Meteorol., 83, 183–205, https://doi.org/10.1023/A:1000268825998, 1997.

Wagner, J. S., Gohm, A., and Rotach, M. W.: The Impact of Horizontal Model Grid Resolution on the Boundary Layer Structure over an Idealized Valley, Mon. Weather Rev., 142, 3446–3465, https://doi.org/10.1175/MWR-D-14-00002.1, 2014.

Wang, C., Jones, R., Perry, M., Johnson, C., and Clark, P.: Using an ultrahigh-resolution regional climate model to predict local climatology, Q. J. Roy. Meteor. Soc., 139, 1964–1976, https://doi.org/10.1002/qj.2081, 2013.

Zardi, D. and Whiteman, C. D.: Diurnal Mountain Wind Systems, in: Mountain Weather Research and Forecasting: Recent Progress and Current Challenges, edited by: Chow, F. K., De Wekker, S. F. J., and Snyder, B. J., Springer Netherlands, Dordrecht, 35–119, https://doi.org/10.1007/978-94-007-4098-3_2, 2013.